Performance of soil-matrix composite reinforced with recycled shredded fibers from waste tires

E. Tolentino[1]*, F. C. de Oliveira[1], L. A. Campos[2], J. Tolentino Junior[3], F. J. H. T. V. Ramos[4]
[1]Federal Centre of Technological Education of Minas Gerais, Timóteo, MG, Brazil
[2]HEAD5 Engenharia, Belo Horizonte, MG, Brazil
[3]Redentor College, Itaperuna, RJ, Brazil
[4]Military Institute of Engineering, Rio de Janeiro, RJ, Brazil

Abstract

Some experimental results concerning the performance of fiber-reinforced soil composites made of soil and shredded fibers from waste tires are presented. The composite mixtures were prepared with fiber addition of 0, 15, 30, and 45 wt%. After molding, the specimens were oven-dried and tested for unconfined compressive strength and water immersion durability. The results showed an improvement in durability with the addition of fiber. The results also indicated good compressive strength performance for the composites with a fiber content of 15 and 30 wt%. The 30 wt% fiber addiction was the best choice because of the environmental sustainability appeal to solid waste reduction.
Keywords: sustainability, shredded waste tires, soil.

INTRODUCTION

One cannot deny that despite advanced modernity's potential to promote humankind's health, the social production of health accompanies the social construction of risks. Risks are the probability of physical harm due to technological or other processes [1]. The growing demand for automobiles has generated an enormous amount of end-of-life tire waste. It is estimated that almost 1000 million tires reach the end of their life each year, and more than 50% of them are discarded without any future use. Recycling tires reduces raw materials consumption, especially those originating from non-renewable resources [2, 3]. The globalization of the building industry caused the extensive application of modern construction techniques and materials to both new and historic buildings. These materials rely heavily on energy-intensive manufacturing procedures and application techniques, and to a great extent, they are responsible for the depletion of the Earth's natural resources. Earth-building technology arises as a feasible alternative for sustainable development. Earth building is the practice of construction using unfired, untreated, raw earth. Earth was the primary material used for building a shelter when men emerged from caves at the dawn of time. Even today, it is estimated that over a third to one-half of the world's population live in some earthen dwelling [4, 5]. The earth has different names when used as a building material, referred to in scientific terms as 'loam', a mixture of clay, silt (fine sand), sand, and occasionally larger aggregates such as gravel or stones. When speaking of compressed unbaked

bricks, 'soil blocks' are used. When compacted within a formwork, it is called 'rammed earth'. 'Mud bricks' or 'adobes' are usually employed when speaking of handmade unbaked bricks. The term adobe originates from the oral form of Spanish/Arabic *al-tob*, meaning, literally, the brick. Earth construction techniques have been known for over 9000 years. Archeologists have discovered mudbrick houses dating from 8000 to 6000 BC in Russian Turkestan. They also found rammed earth foundations dating from ca. 5000 BC in Assyria. Earth was used as the building material in ancient cultures, not only for homes but also for religious buildings. The Temple of Ramses II at Gourna, Egypt, was built from mud bricks 3200 years ago. The 4000-year-old Great Wall of China was initially constructed solely of rammed earth. The core of the Sun Pyramid in Teotihuacan, Mexico, built between AD 300 to 900, consists of approximately 2 million tons of rammed earth [6].

Using soil for construction is cheap, affordable, and easy to use, and it has a high thermal capacity and low thermal conductivity. Thus, soil can moderate extreme outdoor temperatures and maintain a satisfactory internal temperature balance. The disadvantages of using soil for earth-based building materials are its reduced water durability, low tensile strength, and low resistance to abrasion or impact. Several researchers have worked to minimize or eliminate many of these drawbacks. The disadvantages may be overcome by reinforcing the soil mixture with natural or synthetic fibers. The fiber-reinforced soil blocks, rammed-earth, and adobe are soil-matrix composites [7-13]. Natural fibers are found in the environment and are typically extracted from the exterior of plants, trees, and straws. The natural fibers for earth-based building materials production include coir, sisal, palm, jute, flax, straw, bamboo, and sugarcane. Synthetic

* ⓞhttps://orcid.org/0000-0002-7145-1007

fibers are manufactured fibers formed for a purpose, whereas distinct production methods and base material compositions produce synthetic fibers with unique mechanical properties. The synthetic fibers include polypropylene (PP), polyethylene (PE), polyethylene terephthalate (PET), nylon, glass, polyvinyl acetate (PVA), and steel. The use of random discrete flexible fibers in earth-based materials mimics the behavior of plant roots and contributes to the stability of soil mass. Different fibers used as reinforcement in distinctive earth-based materials show countless benefits. These include increased durability, compressive strength, tensile strength, shear strength, elasticity, layer coherence, geometric integrity, thermal properties, reduced shrinkage, reduced formation of cracks, and reduced deadweight due to the lighter weight block. The increase in strength and stiffness was reported to be a function of fiber characteristics, such as aspect ratio, skin friction, weight fraction, and modulus of elasticity. Fiber-reinforced earth-based building materials more often show the development of an increased number of micro-cracks accompanied by more ductile behavior, which can be due to the redistribution of forces within the soil matrix due to the fibers holding parts of the soil matrix at large deformations [13-23].

End-of-life tire waste has demonstrated good recyclability capacity. Generally, three primary materials are produced from it, rubber, steel wires, and textile fibers. The literature shows waste tire rubber's applicability in soil reinforcement and earth-based building materials production. Elastomers used in tires are predominantly physical mixtures of natural rubber (NR) and the copolymer of styrene-butadiene (SBR) and polybutadiene (BR). Two different grinding methods are available to reduce the impact of rubber particle sizes on the mechanical properties of composites, namely, ambient and cryogenic routes. Ambient methods produce a rougher surface of particles, which increases their interaction with the soil matrix when incorporated as reinforcement. There is a current utilization of recycled waste tire crumb rubber, but shredded tire fibers still have little use [17-27]. Although the inclusion of fibers in soil-matrix composites has been the focus of many studies, no comprehensive research optimizes the fiber percentages and relates them to composite strength. Furthermore, there is a scarcity of research that studied the influence of shredded fibers from end-of-life tire waste on the performance of soil-matrix composites. Accordingly, the novelty of the current research resides in incorporating shredded rubber fibers from waste tires into earthen building materials. The research hypothesizes that adding shredded waste tire fibers can enhance the soil-matrix composite's physical and mechanical performance. The objectives of this research were: i) to study and compare the durability in water immersion and the unconfined compressive strength performance of a soil-matrix composite reinforced with shredded waste tire fibers; and ii) to establish the optimum fiber content to achieve high compressive strength performance. The test program involved preparing specimens of four soil-fiber compositions and recording their mechanical and durability performances.

MATERIALS AND METHODS

Soil characterization: the soil was collected from the backside of the Federal Centre of Technological Education of Minas Gerais-CEFET-MG, Timóteo City, Minas Gerais State, Brazil. The word soil has different meanings for different professions, such as agriculturist, geologist, or engineer. From the point of view of an engineer, soil is any uncemented or weakly cemented accumulation of mineral particles formed by the weathering of rocks and the void space between the particles containing water and air. If an excavation is made through the previously undisturbed ground, the following materials are usually encountered: i) topsoil, a layer of organic soil usually not more than 50 cm thick; ii) subsoil, the portion of Earth's crust affected by current weathering; iii) hardpan, a hard rock-like material formed by acid leaching process of iron and alumina oxides; and iv) soil, the soft geological deposits extending from the subsoil to bedrock [28, 29]. Therefore, the soil for this study was taken 60 cm below the natural ground level to avoid the organic matter, confirmed by the absence of the characteristic organic matter's musty smell, which made it suitable for soil-matrix composite production [5]. The soil was collected according to the DNER-PRO 003/94 Brazilian National Department of Roadways standard [30]. The collected soil samples had all lumps broken and material that was not soil, like stones, debris, etc., was removed. The procedure was conducted according to the DNER-ME 041/94 standard [31]. According to the NBR NM 27 Brazilian standard test method [32], the soil samples for analysis were drawn using the quartering method. Quartering is done by dividing the thoroughly mixed sample into four equal parts. The two opposite quarters are discarded, the remaining two quarters are remixed, and the process is repeated until the desired sample size is obtained.

The particle size analysis aims to group the particles into separate ranges of sizes and determine the relative proportion by weight of each size range. The resulting plot is a particle size distribution curve or gradation curve. The soil particle size distribution was determined according to DNER-ME 080/94 standard [33]. The soil's maximum dry density and optimum moisture content were obtained under NBR 7182 standard [34]. The soil moisture content was determined by the oven-dry procedure, according to the NBR 6457 standard [35]. It consisted of taking a soil sample of 300 g, determining its exact weight, drying the sample in an oven at 105-110 °C for 24 h, weighing the sample, and determining the moisture loss by subtracting the oven-dry weight from the moist weight [36]. The soil liquid limit was determined according to the NBR 6459 standard [37]. The soil liquid limit is the moisture content at which the soil changes from plastic to liquid states and begins to flow. It was determined from an apparatus consisting of a semispherical brass cup repeatedly dropped onto a rigid rubber base from a height of 10 mm by a cam-operated mechanism developed by Arthur Casagrande. Dry powder of soil was mixed with distilled water into a paste and placed in the cup to a thickness of 12.5

mm. The soil surface was smoothed, and a groove was cut into the soil using a standard grooving tool. The cam's crank was turned at a rate of 2 revolutions per second, and the number of blows required to close the groove over 12.5 mm was counted and recorded. A soil specimen within the closed portion was extracted to determine the water content. The liquid limit was the water content at which the groove cut into the soil close to over 12.5 mm following 25 blows [36]. The soil plastic limit was determined according to the NBR 7180 standard [38]. The soil plastic limit is the moisture content at which soil begins to crumble when rolled into a thread of about 3 mm in diameter [30].

The chemical composition of the soil samples was evaluated by X-ray fluorescence spectroscopy (XRF, Axios, PanAlytical). X-ray powder diffraction analysis (XRD, AXS D8 Advance Eco, Bruker) was utilized to determine the crystallographic structure of soil samples with CuKα radiation at a voltage of 40 kV and a current of 25 mA. A detector with 192 channels (LynxEye XE) was used at the secondary beam side. Experiments were carried out in a 2θ range of 5-105° with a step size of 0.01° and a counting time of 92 seconds per step. The qualitative interpretation of the diffractogram was performed by comparison with patterns contained in the database PDF 4+ (ICDD, 2014) in Bruker Diffrac.EVA software. The total acquisition time of each diffractogram for this work stage was approximately 30 min. Subsequently, the diagrams were plotted in the Origin program (OringinPro 8, v.1997-2007). Scanning electron microscopy (SEM, Quanta 250 FEG, FEI) was used to generate high-resolution soil images through a field emission gun. This equipment allowed imaging up to 1.5 nm resolution and 1000000x maximum magnification and 30 kV of measurement energy. The Quanta equipment could work under three different pressure ranges, the maximum pressure being 2600 Pa. As soil is a non-conductive material, it was coated with a conductive layer to carry away the electrical charge on the sample surface by absorbing electrons from the primary electron beam. Therefore, a small patch of soil was glued to large SEM stubs, and dried, and its surface was sputter-coated with a conductive layer of a bronze alloy for SEM examination using a high vacuum.

Fibers characterization: Pinho Pneus Co., located in Itaperuna City, Rio de Janeiro State, Brazil, provided samples of shredded fibers from waste tires obtained by grinding tire rubber in special mills. The fibers were subjected to thermal gravimetric (TGA) and differential thermal analysis (DTA). Thermogravimetry measures the mass loss during the decomposition of the sample while heating, whereas differential thermal analysis is a technique for identifying and quantitatively analyzing the chemical reaction of substances by observing the thermal behavior as it is heated. For thermal analysis (DTG-60, Shimadzu), samples of 10 mg were placed in a platinum crucible and heated from 20 up to 600 °C at 10 °C/min. The tests were performed under a 60 mL/min nitrogen flow, and the reference material used for measurements was α-alumina. SEM (Quanta 250 FEG, FEI) was used to obtain fiber images. A fiber sample was glued on a large SEM stub and dried. Its surface was sputter-coated with a conductive layer of gold-palladium alloy for SEM examination using a high vacuum.

Molding and drying operations of cylindrical specimens: specimens of 50 mm diameter and 100 mm height with a slenderness ratio (ratio between height and width) of 2:1 were molded and oven-dried. The minimum size required for static testing on masonry components is 40 mm, according to EN 772-1:2000 standard [39]. The tire fibers were weighted according to the percentage ratio of soil weight. Four materials proportions for this study were prepared to incorporate different fiber dosages: 0, 15, 30, and 45 wt%. Good workability and plasticity are essential to obtaining a quality finished product. The water is required to activate the bond strength and achieve workability, but too much water may cause damage because drying cause significant axial shrinkage. Therefore, the specimens were molded with the quantity of water of one-quarter dry soil weight [9-11], using tap water provided by the COPASA, the Water and Sanitation Public Utility Company of Minas Gerais State. The soil was air-dried at the laboratory's environmental conditions of 23 °C and 66% RH, before Atterberg limits tests and soil-fiber blending procedures. The mixing of materials and compaction of cylindrical specimens were manual. The fibers were added gradually to the soil to reduce the formation of fiber clusters. Once the fibers were incorporated into the mixture, the water was added. The water proportion was chosen according to the obtained results of the optimum moisture content value, which corresponded to the maximum dry unit weight of clayey soil. The total number of molded specimens for each mixture was eight. After the molding operation, a soil sample was collected from one specimen of each mixture proportion for moisture content and dry unit weight check to determine the relative compaction of the soil. The specimens were demolded 24 h after molding. Half of the molded specimens for each mixture were heat-treated by oven-drying (Biopar) at 150 °C for 24 h. Drying time and temperature are critical factors in retaining the soil-matrix composites' strength and avoiding cracks or fractures. The choice of oven-drying temperature for this study was according to references [13, 20, 40]. The heat-treated and non-heat-treated specimens were wrapped in plastic to prevent water loss and were kept in the laboratory for 28 days before the characterization testing program.

Testing of cylindrical specimens: the specimens were subjected to static tests, according to EN 772-1:2000 standard [39], using a universal testing machine (AG-X-V, Shimadzu). Two special compression platens of 115 mm diameter were used to load the specimens in compression correctly, and the displacement was controlled at a constant velocity of 2 mm/min. The specimens were further subjected to a water immersion test, an accelerated aging test that allowed obtaining information about durability. The test consisted of immersing the specimens in water for 5 h at room temperature, according to DNER-ME 256/94 standard [41].

RESULTS AND DISCUSSION

Soil particle size distribution, liquid limit, and plastic limit: Fig. 1 shows the particle size distribution data of the soil sample. It gives information on soil's ability to pack into a dense structure, providing initial rough estimates of its engineering properties such as permeability, strength, and expansivity [11]. Soils with an even distribution of grain sizes are called well-graded. The continuous grading curve of well-graded soils traverses several particle sizes ranges [42]. Soils with an excess or deficiency of specific particle sizes, or soil with at least one particle size missing, are named gap-graded soils. Gap-graded soils tend to retain the memory of their initial distribution even after compression to high stress. The grain size distribution curve shows a 'knee' corresponding to the size of small particles in the gap-graded soil [43]. The results revealed a continuous particle size distribution characteristic of well-graded soils, so the soil needed no correction in the particle size matter [44]. Many particle sizes do not have their representation in the soil curve shown in Fig. 1 because these sized particles are not present in the soil sample. In addition to the visual analysis of the particle size distribution curves, the coefficient of curvature (Cc) helps classify the soil. The coefficient of curvature (Cc) should lie between 1 and 3 for well-graded soil, according to [45]:

$$Cc = \frac{D30^2}{D60 \cdot D10} \tag{A}$$

where D60 is the particle size at 60% finer, D30 is 30% finer, and D10 is 10% finer. As the calculation result of this study was 2, the analyzed soil was confirmed as well-graded.

Table I reports the results of soil elements, hygroscopic moisture content, liquid limit, and plastic limit. The sieve analysis results showed the soil was composed of 22.2% medium sand, 33.6% fine sand, and 44.2% clay plus silt. Additionally, the obtained results of the liquid limit, plastic limit, and plasticity index were 14.5%, 1.6%, and 12.9%, respectively. So, it is an A-6 clayey soil, according to the Highway Research Board (HRB) classification [36]. There are different recommendations for soil particle sizes suitable for various earth-building techniques. Clay and silt, cohesive elements in nature, form a matrix in which the sand particles are enclosed, acting as a binder for the cohesionless granular fraction of the soil. It is supposed to strengthen the dried material. According to the literature [10-12, 28], the results showed that the soil element proportion was appropriate for earth construction.

Soil chemical characterization: the oxide composition of the soil sample obtained by XRF is given in Table II. In Fig. 2, the XRD diffractogram is reported. The mineralogical characterization of the soil obtained by XRD revealed that its main components were halloysite-7 Å and halloysite-10 Å [$Al_2(Si_2O_5)(OH)_4$], and kaolinite [$Al_2(Si_2O_5)(OH)_4$], and minor components as goethite [α-$Fe^{3+}O(OH)$], quartz (SiO_2), iron oxide (FeO), among others. Halloysite and kaolinite are dioctahedral 1:1-layer hydrated aluminum silicates. They have the same chemical composition, except that halloysite has higher water content. Both are alterations of feldspars due to the differences in the activities of K^+, Al, H_4SiO_4, and H^+ in the environments. The porosity of the soil-matrix composite is strongly related to the silica content in the mix, and the alumina content improves soil-matrix composite performance. The iron oxide may often cause efflorescence, provided the content is more than 10 wt%. Therefore, according to the literature [13], the XRF analysis showed that the three chemical components, silica, alumina, and iron oxide, were in the appropriate range for soil-matrix composite production.

Soil image analysis: Fig. 3 shows the SEM image of a piece of the soil sample. Table III presents the composition
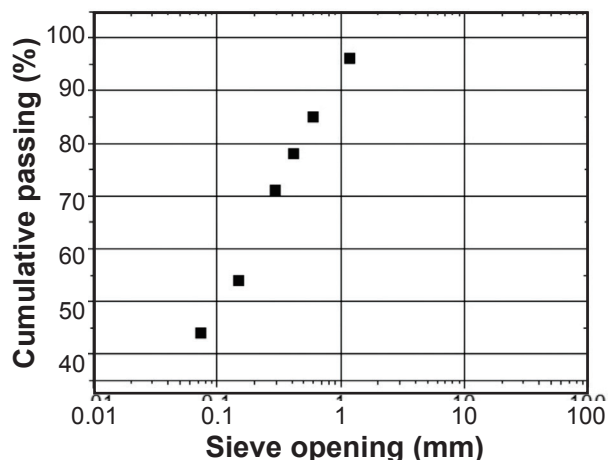
Figure 1: Particle size distribution data of the soil sample.

Table I - Soil granulometry, hygroscopic moisture content, liquid limit, and plastic limit.

Soil granulometry		Hygroscopic moisture content (%)	Liquid limit (%)	Plastic limit (%)
Clay+silt content (%)	Medium+fine sand content (%)			
44.2	55.8	2.1	14.5	1.6

Table II - Chemical composition (wt%) measured by XRF of the studied soil sample.

SiO_2	Al_2O_3	K_2O	Fe_2O_3	MgO	Na_2O	TiO_2	LOI*
57.50	30.70	4.90	0.79	0.25	0.23	0.13	5.50

*: loss on ignition.
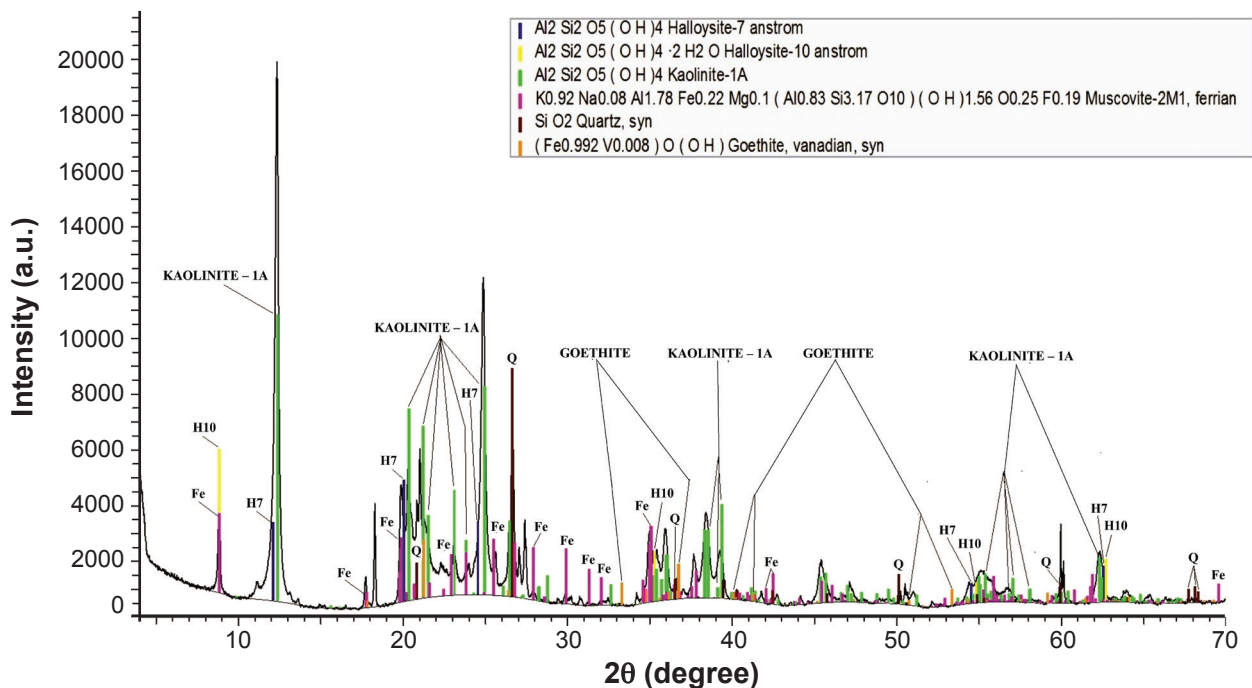
Figure 2: XRD diffractogram of the soil sample.

of the elements obtained by SEM-EDS (energy dispersive spectroscopy) of the soil sample at the square region indicated in Fig. 3a. The sample's analysis of a particle field revealed the typical elements of an altered feldspar [46]. The presence of tin (Sn) and copper (Cu) was due to sampling preparation with bronze alloy for SEM analysis. The presence of hafnium (Hf) was likely due to contamination or the coincidence of peaks.

Shredded tire thermal analysis: Fig. 4 shows the decomposition processes of the shredded tire fiber sample. TGA curve showed a slight weight loss until around 300 °C, which was due to the volatilization of chemical additives such as plasticizers and processing oils in the tire. Then, from 300 up to 570 °C, the weight loss associated with the rubber degradation was observed. The DTA curve indicated distinct peaks at about 420, 480, and 490 °C, corresponding

Table III - Chemical composition of elements (wt%) measured by SEM-EDS of the studied soil sample at the square region indicated in Fig. 3a.

Element	Atomic number	Content (wt%)
O	8	31.2±3.4
Cu	29	21.2±0.5
C	6	12.8±1.9
Hf	72	12.8±0.3
Al	13	9.52±0.44
Si	14	7.35±0.31
Fe	26	3.69±0.12
Sn	50	1.43±0.07
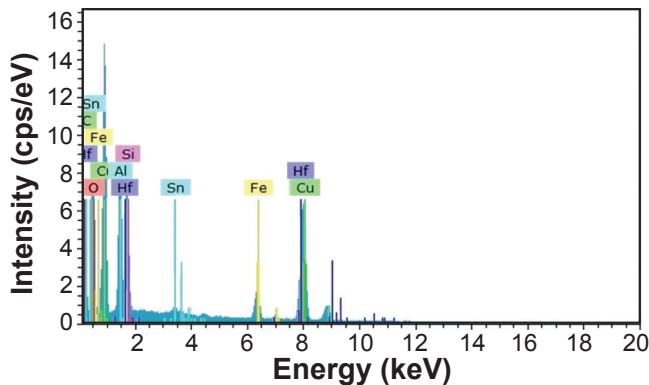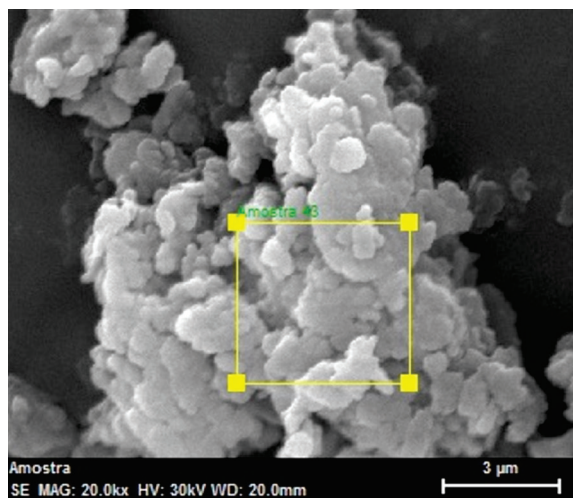
Figure 3: SEM image of soil sample (a) and EDS spectrum of the square region indicated in 'a' (b).
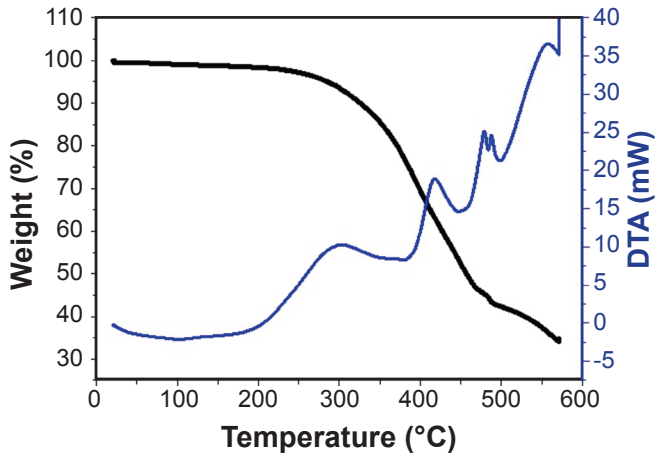
Figure 4: DTA and TGA curves of the shredded tire fiber sample.

to the degradation of the major rubber components of the tire, such as styrene-butadiene rubber (SBR), natural rubber (NR), and polybutadiene rubber (BR) [21, 40, 47, 48].

Shredded tire fiber image analysis: Fig. 5 presents photographic images and a SEM image of shredded fibers of waste tires. The SEM image revealed the shredded fiber surface was not smooth and did not have a uniform thickness. The confidence interval for the population mean of the shredded fibers sample's length, diameter, and aspect ratio (mean±standard deviation) were 18.5±1.3 mm, 1.6±0.2 mm, and 11.9±2.5, respectively. For a significance level of 0.05 and 9 degrees of freedom, the critical value for the t-test was 2.262. Fig. 6 presents SEM images of shredded tire fiber, showing the rough surface of the fiber. The surface appearance of fiber was explained by the grinding process in special mills to which fibers were submitted. According to the literature, the composite's mechanical properties strongly rely on the behavior and interaction of the fiber with the parent matrix interface. The interfacial adhesion stems from fiber-matrix mechanical interlocking, and a solid interfacial adhesion guarantees efficient load transfer from the soft soil matrix to stiff fibers. The shear resistance of the soil governs adhesion at the fiber-matrix interface due to the surface form and roughness of the fiber and the compressive friction forces on the fiber's surface due to the shrinkage of the soil. The enhancing effect of interface roughness on the composite's mechanical properties is only significant for fibers with a small and medium aspect ratio [15-18, 49].

Cylindrical specimens water immersion test: Fig. 7 shows the water immersion test of four heat-treated fiber-reinforced soil composites, incorporating different fiber dosages of 0, 15, 30, and 45 wt%. The test compared the relative performance of the composites after submerging them continuously for 5 h. In a composite, the matrix material should be ductile, and in addition, the elastic modulus of the fiber should be much higher than that of the matrix. The results revealed that the fiber-reinforced soil composites performed better than the non-fibered sample, confirming that fibers bound the soil matrix together. Furthermore, the observed effect was ascribed to the hydrophobic nature of the shredded tire rubber, which dramatically reduced the net force
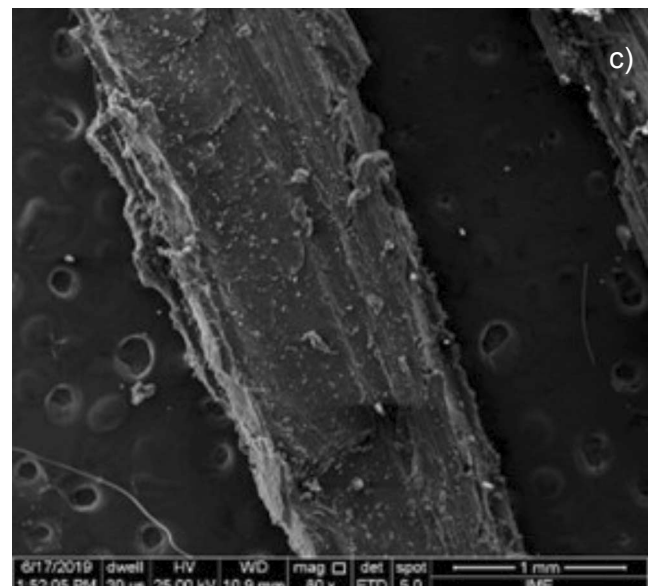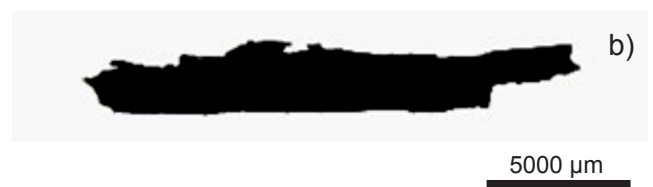
Figure 5: Images of fibers of waste tires: a) photographic image of shredded fibers as received; b) photographic image of one shredded fiber; and c) SEM image of shredded fiber.
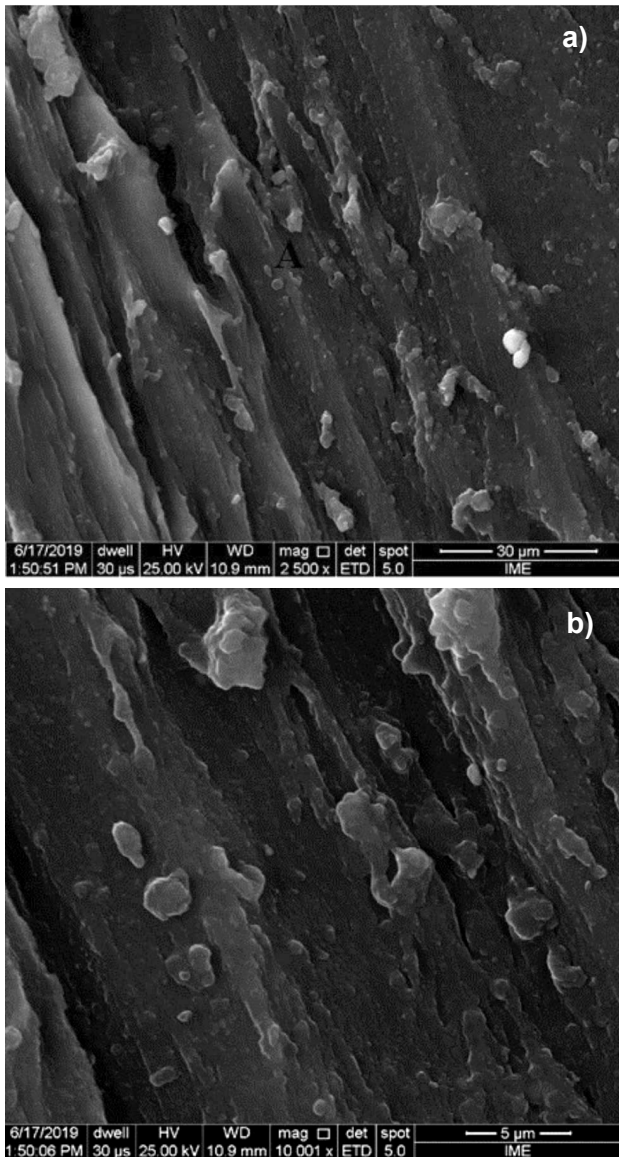
Figure 6: SEM images of shredded tire fiber at different magnifications
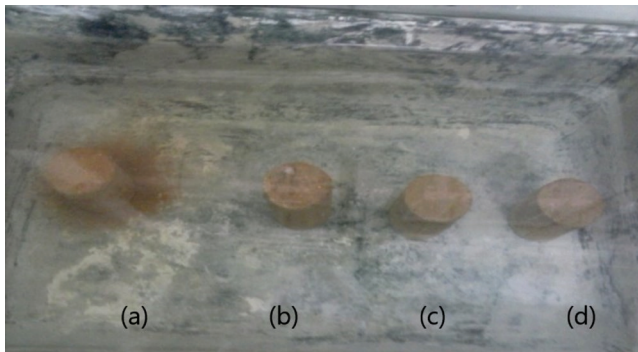
Figure 7: Heat-treated cylindrical specimens subjected for 5 h of water immersion test with a fiber content of: a) 0 wt%; b) 15 wt%; c) 30 wt%; and d) 45 wt%.

for water penetration in the composites [18, 24, 49, 50].

Cylindrical specimens image analysis: Fig. 8 shows SEM images of the soil matrix of the 30 wt% fiber-reinforced composite specimen. The presence of halloysite with its typical tubular morphology and elongated *habitus* was observed. On the report of other researchers, kaolin is a rock formed by a group of hydrated aluminum silicates. Kaolin presents mainly kaolinite crystals with varying levels of halloysite-7 Å/10 Å. Impurities such as sand, quartz, mica, feldspar grains, iron, titanium oxides, etc., are also present. Kaolinite crystals have lamellar morphology and irregular profile, rarely hexagonal. Halloysite is of the 7 Å or $2H_2O$ type with tubular morphology. Such presence in soil composite matrix samples was because the oven-drying temperature could not degrade the halloysite crystals but only dehydrate them [51-57].

Cylindrical specimens compressive strength test: Table IV presents the sample mean, standard deviation, and confidence interval of the population mean for the unconfined compressive strength of soil-fiber reinforced
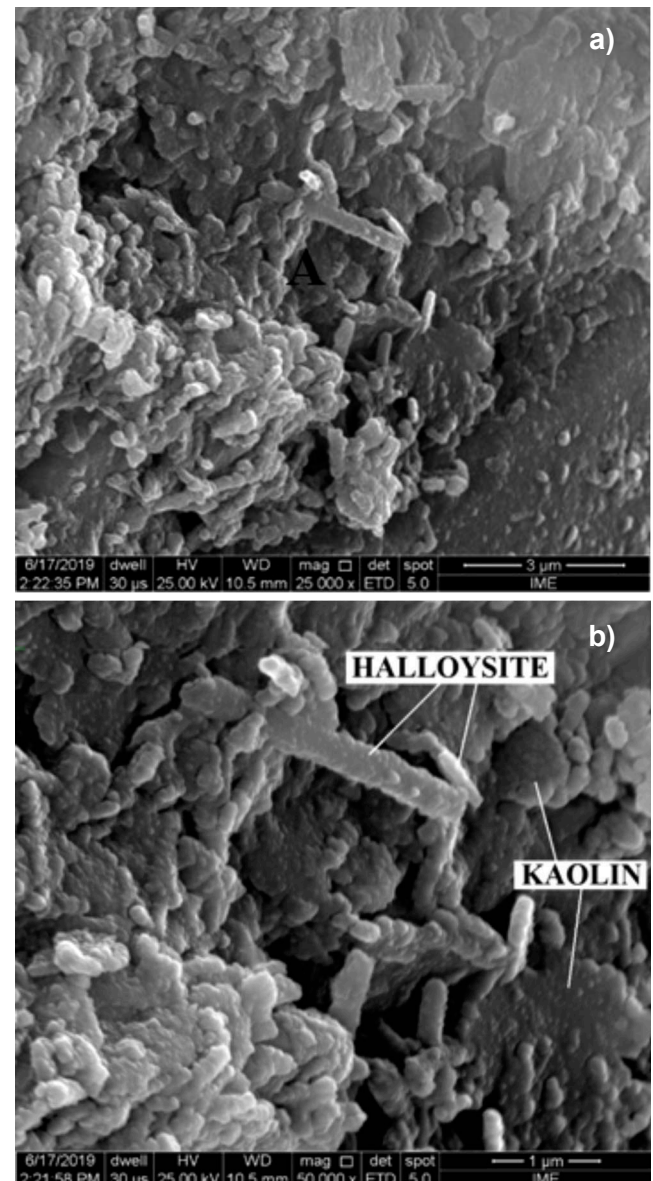
Figure 8: SEM images of soil matrix of the 30 wt% fiber-reinforced composite at different magnifications.

Table IV - Compressive strength of soil-fiber reinforced composite specimens (MPa): mean±standard deviation and confidence interval.

0NHT	0HT	15NHT	15HT	30NHT	30HT	45NHT	45HT
0.79±0.05	0.84±0.03	0.91±0.04	0.97±0.12	0.87±0.02	0.91±0.02	0.71±0.03	0.80±0.03
$0.72 \leq \mu \leq 0.80$	$0.80 \leq \mu \leq 0.87$	$0.85 \leq \mu \leq 0.96$	$0.80 \leq \mu \leq 1.14$	$0.85 \leq \mu \leq 0.90$	$0.88 \leq \mu \leq 0.93$	$0.68 \leq \mu \leq 0.75$	$0.76 \leq \mu \leq 0.85$

NHT: non-heat-treated; HT: heat-treated; the number (0, 15, 30, 45) indicates the fraction (wt%) of fiber added to the composite.

composite specimens. The degree of freedom of all tests was 3. One can note that heat treatment improved the compressive strength performance of composites. It was also noted that as the fiber content increased, the compressive strength increased to a specific value and gradually decreased. According to other researchers, the fiber properties are governed by the chemistry of the polymer chains and the fiber drawing process. The increase in compressive strength with fiber addition was because of the fiber's reinforcement action and their small aspect ratio and rough surface, as shown in Figs. 5 and 6. Developing fiber-reinforced soil composite strength largely depends on forming fiber-matrix, matrix-matrix, and fiber-fiber bonds. The number of contact points between fibers and the soil matrix is responsible for transmitting stress. A large number of fibers, therefore, reduced the strength of earthen blocks. As the percentage of fibers present in matrices increased, the volume of the soil-matrix confining each fiber strand decreased, and there was more fiber-fiber interaction, which did not result in the formation of bonds and led to less bond-forming fiber-matrix interaction [14, 15, 49].

Determining the optimum fiber content to achieve the best compressive strength performance: the statistical analyses were performed using the Minitab 16 software. Fig. 9 shows the main effects plot for mean compressive strength results of the fiber-reinforced soil composites. The right curve presents the fiber content effect, and the curve on the left shows the heat-treatment effect. When analyzing the main effects graph, it was found that the heat treatment positively affected the mechanical performance of the composites. It was also noticeable that there was an increase in the compressive strength of the composites with a polymeric fiber content of 15 and 30 wt%, with the best result obtained for the 15 wt% fiber-content composite. The worst result was for the composites with a fiber dosage of 45 wt%. It was attributed to the difficulties faced in the raw materials mixing stage and the fiber-fiber interaction [14, 15, 49]. Fig. 10 shows the normal probability plot of residuals, which is a way of learning whether it is reasonable to assume that the error terms are normally distributed. The plot showed that normality was probably a reasonably good approximation because the data tended to be a straight line [57]. Fig. 11 presents the interaction plot for mean compressive strength results data. The results showed that the composite with a fiber content of 15 wt% had the best strength performance when comparing heat-treated and non-heat-treated conditions.

Fig. 12 shows the linear regression analysis to investigate the relationship between compressive strength results and fiber content. A P-value lesser than 0.05 indicates whether these relationships are statistically significant in this context. The P-value was 0.00, proving the statistically significant relationship between compressive strength results and fiber content. The regression model could account for the 69.78% result of variation for the compressive strength. The fitted equation for the cubic model that described the relationship between compressive strength results and fiber
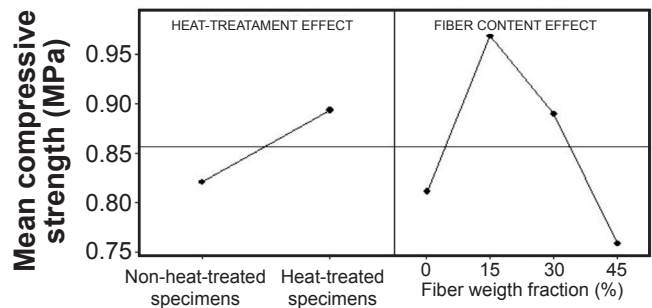
Figure 9: Main effects plot for mean compressive strength results.
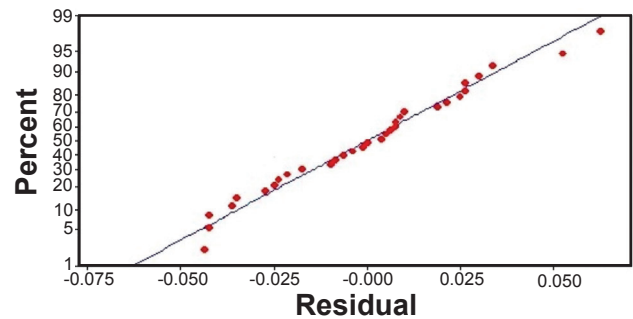
Figure 10: Normal probability plot of residuals.
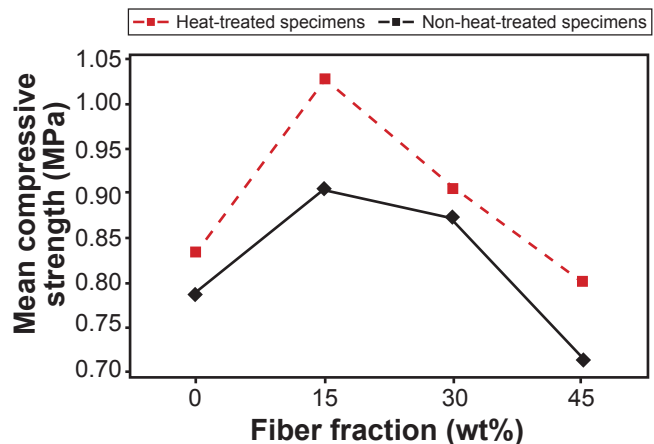
Figure 11: Interaction plot for mean compressive strength data.

percentages is given by:

$$Y = 0.8114 + 0.02238.X - 0.000931.X^2 + 0.000009.X^3 \quad (B)$$

where Y is the compressive strength and X is the fiber percentage content. The results showed a tendency to obtain statistically favorable compressive strength results for the composites manufactured with the shredded fibers from waste tire content of 15 and 30 wt%. Besides, there was a smaller disparity between compressive strength results for composites made with a 30 wt% addition of fibers.
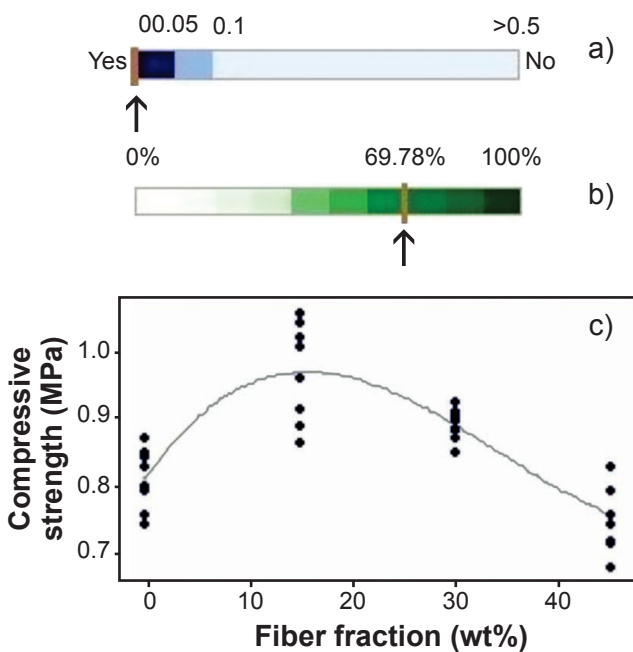
Figure 12: Results of linear regression analysis for mean compressive strength results and fiber content: a) P-value as indicated by an arrow; b) percent of variation accounted by the model as indicated by an arrow; and c) fitted equation plot for the cubic model.

CONCLUSIONS

The current work investigated the possibility of reusing shredded waste tire fibers as reinforcement in soil-matrix composites. Based on the available test results and analysis, the following conclusions could be drawn: 1) the incorporation of shredded waste tire fiber in soil-matrix composites reduced the net force for water absorption, increasing its durability; and 2) the best choice for optimum shredded waste tire fiber content was 30 wt% as soil matrix reinforcement because of the smaller disparity between compressive strength results and the environmental sustainability appeal to solid waste reduction.

ACKNOWLEDGMENTS

REFERENCES

[1] U. Beck, *Risk society: towards a new modernity*, Sage Publ., London (1992).
[2] J. Svoboda, V. Vaclavik, T. Dvorsky, L. Klus, R. Zajac, in Proc. Construmat, Slovakia (2018) 1.
[3] P. Sharma, A. Sharma, A. Sharma, P. Srivastava, Res. J. Chem. Environ. Sci. **4**, 2 (2016) 1.
[4] R. Illampas, I. Ioannou, D.C. Charmpis, in Proc. 4th Int. Conf. Sustain. Develop. Plann., C.A. Brebbia, M. Neophytou, E. Beriatos, I. Ioannou, A.G. Kungolos (Eds.), Cyprus (2009) 245.
[5] C. Bock-Hyeng, A.N. Ofori-Boadu, E. Yamb-Bell, M.A. Shofoluwe, Int. J. Eng. Res. Appl. **6**, 9 (2016) 50.
[6] G. Minke, *Building with earth*, Birkhäuser Basel, Berlin (2006).
[7] E.A. Adam, A.R.A. Agib, *Compressed stabilized earth block manufacture in Sudan*, UNESCO, Paris (2001).
[8] G. Calatan, A. Hegyi, C. Dico, C. Mircea, Procedia Technol. **22** (2016) 259.
[9] A. Revuelta-Acosta, G.M. Garcia-Diaz, J. Appl. Sci. **10** (2010) 2011.
[10] D. Benghida, Adv. Mater. Res. **1105** (2015) 386.
[11] H. Danso, Adv. Civ. Eng. Tec. **2** (2018) 199.
[12] T.L. Piani, D. Krabbenborg, J. Weerheijm, L. Koene, L.J. Sluijs, J. Green Build. **13**, 3 (2018) 17.
[13] M.M. Salih, A.I. Osofero, M.S. Imbabi, Struct. Civ. Eng. **14**, 4 (2020) 839.
[14] M. El-Emam, A. Al-Tamimi, Sustainability **14**, 4850 (2022) 1.
[15] P. Donkor, E. Obonyo, C. Ferraro, Materials **14**, 6906 (2021) 1.
[16] J. Concha-Riedel, F.C. Antico, G. Araya-Letelier, Rev. Matér. **25**, 4 (2020) 1.
[17] S.M. Hejazi, M. Sheikhzadeh, S.M. Abtahi, A. Zadhoush, Const. Build. Mater. **30** (2012) 100.
[18] A. Mohajerani, S.Q. Hui, M. Mirzababaei, A. Arulrajah, S. Horpibulsuk, A.A. Kadir, Md.T. Rahman, F. Maghool, Materials **12**, 2513 (2019) 1.
[19] M. Bekhiti, G. Abderrahmane, R. Zaitri, J. King Saud Univ. Eng. Sci., *in press*.
[20] B. Acevedo, A.M. Fernández, C. Barriocanal, J. Anal. Appl. Pyrolysis **111** (2015) 224.
[21] S. Kordoghli, M. Paraschiv, R. Kuncser, M. Tazerout, M. Prisecaru, F. Zagrouba, I. Georgescu, J. Eng. Stud. Res. **20**, 4 (2014) 1.
[22] V. Sharma, H.K. Vinayak, B.M. Marwaha, Int. J. Sustain. Built Environ. **4** (2015) 348.
[23] M.M. Kamal, M.A. Safan, Z.A. Etman, R.A. Salama, HBRC J. (2013) 1.
[24] A. Petrella, R. Di Mundo, S. De Gisi, F.T.C. Labianca, M. Notarnicola, Materials **12** (2019) 3289.
[25] S.E. Kelechi, M. Adamu, A. Mohammed, Y.E. Ibrahim,

I.I. Obianyo, Materials **15**, 455 (2022) 1.

[26] F.C. Cabrera, Polym. Compos. **42** (2021) 2653.

[27] M. Abbaspour, E. Aflaki, F.M. Nejad, J. Clean. Prod. **207** (2019) 1059.

[28] G.N. Smith, I.G.N. Smith, *Elements of soil mechanics*, John Wiley Sons, Oxford (1998).

[29] R.F. Craig, *Craig's soil mechanics*, Spoon Press, London (2004).

[30] DNER PRO 003/94, "Collecting deformed soil samples", Braz. Natl. Dept. Rwy. Stand., Mato Grosso (1994).

[31] DNER ME 041/94, "Soils: preparation of samples for characterization tests", Braz. Natl. Dept. Rwy. Stand., Rio Janeiro (1994).

[32] ABNT NBR NM 27, "Field sample reduction for laboratory testing", Braz. Ass. Tech. Stand., Rio Janeiro (2001).

[33] DNER ME 080/94, "Soils: grain size analysis by sieving", Braz. Natl. Dept. Rwy. Stand., Rio Janeiro (1994).

[34] ABNT NBR 7182, "Soil: compaction test", Braz. Ass. Tech. Stand., Rio Janeiro (2016).

[35] ABNT NBR 6457, "Soil samples: preparation for compaction tests and characterization tests", Braz. Ass. Tech. Stand., Rio Janeiro (1986).

[36] H.P. Caputo, *Mecânica dos solos e suas aplicações*, LTC, Rio Janeiro (1996).

[37] ABNT NBR 6459, "Determining liquid limits of soils", Braz. Ass. Tech. Stand., Rio Janeiro (1984).

[38] ABNT NBR 7180, "Determining plastic limits of soils", Braz. Ass. Tech. Stand., Rio Janeiro (1984).

[39] BS EN 772-1, "Methods of test of masonry units: determination of compressive strength", Brit. Stand. Inst., London (2000).

[40] S.S. Moulin, A. Bounaceur, M. Herblot, Y. Soudais, Waste Biomass Valori. **8**, 8 (2017) 2757.

[41] DNER ME 256/94, "Compacted soils with miniature equipment: determination of mass loss by immersion", Braz. Natl. Dept. Rwy. Stand., Rio Janeiro (1994).

[42] Y. Nakata, M. Hyodo, A.F. Hyde, Y. Kato, H. Murata, Soils Found. **41**, 1 (2001) 69.

[43] X. Zhang, B.A. Baudet, W. Hu, Q. Xu, Soils Found. **57** (2017) 603.

[44] J.S. Nogami, D.F. Villibor, in Proc. Braz. Symp. Trop. Soils Eng., Rio Janeiro (1981) 30.

[45] ASTM, in "Annual book, Sect. 4, Construction", 04.08, ASTM Int., Philadelphia (1990).

[46] J.D. Dana, *Manual de mineralogia*, LTC, Rio Janeiro (1981).

[47] P.T. Williams, S. Besler, Fuel **74**, 9 (1995) 1277.

[48] D. Czajczyńska, K.M. Czajka, R. Krzyżyńska, H. Jouhara, E3S Web Conf. **100** (2019) 12.

[49] Y. Yao, S. Chen, J. Compos. Mater. **47**, 23 (2012) 2909.

[50] W.D. Callister, *Materials science and engineering: an introduction*, John Wiley Sons, New York (2007).

[51] P. Souza Santos, in Proc. 2nd World Cong. Non-ME Miner., Beijing (1989) 176.

[52] P. Souza Santos, in Proc. 2nd World Cong. Non-ME Miner., Beijing (1989) 497.

[53] P. Souza Santos, *Ciência e tecnologia de argilas*, Edgard Blücher, S. Paulo (1975).

[54] P. Souza Santos, Clay Miner. **28** (1993) 539.

[55] G.W. Brindley, P. Souza Santos, H. Souza Santos, Am. Mineral. **48**, 3 (1963) 897.

[56] J. Tolentino Junior, "Potencial dos depósitos de caulim halloysítico associados aos pegmatitos da região de Juiz de Fora visando o seu aproveitamento econômico", PhD Thesis, State Univ. Rio Janeiro (2019).

[57] D.C. Montgomery, *Design and analysis of experiments*, John Wiley Sons, New York (1997).